

Prediction of freestanding semiconducting bilayer borophenes

Yuan-Yuan Ma^{1,2}, Xiao-Yun Zhao³, Wenyan Zan¹, Yuewen Mu¹ (✉), Zhuhua Zhang⁴ (✉), and Si-Dian Li¹ (✉)

¹ Institute of Molecular Science, Shanxi University, Taiyuan 030006, China

² FenYang College of Shanxi Medical University, FenYang 032200, China

³ Department of Applied Chemistry, Yuncheng University, Yuncheng 044000, China

⁴ State Key Laboratory of Mechanics and Control of Mechanical Structures, and Key Laboratory for Intelligent Nano Materials and Devices of Ministry of Education, Nanjing University of Aeronautics and Astronautics, Nanjing 210016, China

© Tsinghua University Press 2022

Received: 10 November 2021 / Revised: 24 December 2021 / Accepted: 17 January 2022

ABSTRACT

Supported bilayer α -borophene (BL- α borophene) on Ag(111) substrate has been synthesized in recent experiments. Based on the experimentally observed quasi-planar C_{6v} B_{36} (**1**), its monolayer assembly α^* -borophene B_{11} (*P6/mmm*) (**2**), and extensive global minimum searches augmented with density functional theory calculations, we predict herein freestanding BL- α^* borophenes B_{22} (*Cmmm*) (**3**) and B_{22} (*C2/m*) (**4**) which, as the most stable BL borophenes reported to date, are composed of interwoven boron triple chains as boron analogs of monolayer graphene (**5**) consisting of interwoven carbon single chains. The nearly degenerate eclipsed B_{22} (**3**) and staggered B_{22} (**4**) with the hexagonal hole density of $\eta = 1/12$ and interlayer bonding density of $u = 1/4$ appear to be two-dimensional semiconductors with the indirect band gaps of 0.952 and 1.144 eV, respectively. Detailed bonding analyses reveal one delocalized 12c-2e π bond over each hexagonal hole in both the B_{22} (**3**) and B_{22} (**4**), similar to the situation in monolayer graphene which contains one delocalized 6c-2e π bond over each C_6 hexagon. Furthermore, these BL- α^* borophenes appear to remain highly stable on Ag(111) substrate, presenting the possibility to form supported BL- α^* borophenes.

KEYWORDS

boron nanomaterials, bilayer borophenes, structures, bonding, semiconductors

1 Introduction

Graphene, a honeycomb monolayer (ML) allotrope of carbon composed of interwoven carbon single chains (CSCs), has played an essential role in nanoscience and technology ever since its experimental preparation [1]. As a typical Dirac material [2], graphene has exhibited huge advantages to operate in electronic, magnetic, optical, thermoelectric, catalysis, and energy storage systems. Other ML two-dimensional (2D) materials such as silicene [3–5], BN monolayers [6, 7], phosphorene [8], and MoS₂ sheets [9, 10] with particular properties and significant potential applications have also been synthesized in recent years. As the light neighbor of carbon in the periodic table, boron exhibits strong propensity to adopt sp² hybridizations which result in various planar boron clusters [11, 12], cage-like borospherenes [13, 14], and low-dimensional boron nanomaterials [15–17]. In particular, the experimentally observed quasi-planar boron cluster C_{6v} B_{36} (**1**) which is dually π -aromatic in nature analogous to coronene $C_{24}H_{12}$ (**6**) has been employed as building blocks to form the most stable ML α -boron sheet named borophene [18–20]. ML α -boron sheet with a hole density of $\eta = 1/9$ appears to be π -isovalent with that of ML graphene, with one 6c-2e π bond over each B_6 hexagonal hole and one 7c-2e π bond over each B-centered B_7 hexagon [19, 21–23]. The stability of ML borophenes depends heavily on their hole density, preferably in a range of $\eta = 1/9$ –1/7 [24–28]. Various supported ML borophenes like β_{12} , χ_3 ,

and α -sheet have been synthesized in recent years on Ag, Au, Cu, and Ni substrates which are known to be the thinnest metallic materials ever reported [16, 29–31]. However, there have been no freestanding ML borophenes realized to date in experiments due to their high reactivity in atmospheres, strong adhesion on substrates, and tendency to form interlayer bonding interactions.

Previous theoretical investigations have shown that the formation of bilayer (BL) borophenes passivated on the inner side can effectively stabilize the systems [32–34]. Zhou et al. predicted the BL borophene B_8 (*Pmmm*) [32] made of buckled triangular layers which appeared to be about 50 meV/atom more stable in energy than the most stable ML α -sheet and its analogues. The first supported BL semiconducting α -borophene B_{16} (BL- α borophene) deposited on Ag(111) substrate with a hole density of $\eta = 1/9$ and interlayer bonding density of $u = 2/9$ was recently realized in a molecular beam epitaxy (MBE) experiment [35]. However, such supported BL- α borophenes are expected to be unstable when peeled off from the metal substrate (Fig. S1(a) in the Electronic Supplementary Material (ESM)). Large-size, single-crystalline bilayer borophene was also very recently synthesized on Cu(111) surface by MBE [36] (Fig. S1(b) in the ESM). However, to our best knowledge, stable, freestanding BL borospherenes of great potential for applications in functional devices still remain elusive in both experiments and theory.

Using the experimentally observed quasi-planar C_{6v} B_{36} (**1**) as building blocks to form the self-assembled ML- α^* borophene B_{11}

Address correspondence to Yuewen Mu, ywmu@sxu.edu.cn; Zhuhua Zhang, chuwazhang@nuaa.edu.cn; Si-Dian Li, lisidian@sxu.edu.cn

($Cmmm$) (2) and based on extensive global minimum (GM) searches and density functional theory (DFT) calculations, we find in this work free-standing BL semiconducting α^+ -borophenes B_{22} ($Cmmm$) (3) and B_{22} ($C2/m$) (4) consisting of interwoven boron triple chains (BTCs) with $\eta = 1/12$ and $u = 1/4$, respectively. These BL- α^+ borophenes as the most stable free-standing BL borophenes reported so far possess a delocalized 12c-2e π -bond over each B_6 hexagonal hole, forming a unique π -system analogous to that of the ML graphene which contains a delocalized 6c-2e π -bond over each C_6 hexagonal hole. Such BL- α^+ borophenes are found to be obviously more stable than the previously reported BL- α borophene on Ag(111) substrate [35].

2 Theoretical procedures

Extensive GM searches on BL borophenes with hole densities between $\eta = 0\text{--}0.25$ were carried out using the alloy theoretical automated toolkit (ATAT [37]) based on the cluster expansion (CE) method [38], with the B_6 hexagonal vacancies (Vac) dealt as dopants. Complementary structural searches were performed using the CALYPSO code [39] with the local particle swarm optimization (PSO) minimization scheme within the unit cells containing 16, 18, 20, 22, 24, 26, 28, 30, 32, and 34 atoms, respectively. Local structural relaxations were performed using density functional theory within the Perdew–Burke–Ernzerhof (PBE) parametrization of generalized gradient approximation (GGA) [40], as implemented in the Vienna *ab initio* simulation package (VASP) code [41, 42]. The PBE functional has been confirmed to perform well for boron systems [43]. A dispersion correction of total energy (DFT-D3 method) [44] was used to incorporate the long-range van der Waals interaction. A vacuum slab of 20 Å was selected and a plane-wave basis set with an energy cutoff of 500 eV was used. The electron localization functions (ELF) [45, 46] of optimized BL borophenes were calculated at PBE level using the VASP code with Monkhorst–Pack k-point meshes of $13 \times 13 \times 1$, with their band structures and projected densities of states (PDOS) obtained at the more accurate Heyd–Scuseria–Ernzerhof (HSE06) hybrid functional level [47]. To check the dynamical stability of the obtained B structures, phonon dispersion analyses were performed using the finite displacement method [48] as implemented in the Phonopy code [49], interfaced with the density functional perturbation theory [50] as implemented in VASP. In phonon calculations, a plane wave energy cut-off of 500 eV was employed with more stringent convergence criteria for energy (10^{-8} eV) and force (0.0001 eV/Å). *Ab initio* molecular dynamics (AIMD) simulations with canonical ensemble were performed to evaluate the dynamic stability of the systems [51, 52]. Bonding analyses were done using the solid state adaptive natural density partitioning (SSAdNDP) method [53] which revealed both the localized and delocalized bonds in concerned systems. The SSAdNDP results were visualized using the VMD 1.9.3 program [54].

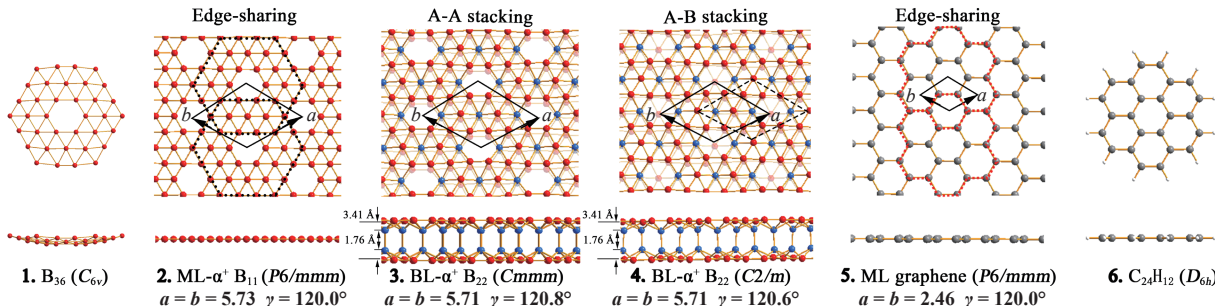


Figure 1 Top and side views of the optimized structures of quasi-planar C_{6v} B_{36} (1), ML- α^+ borophene B_{11} ($P6/mmm$) (2), eclipsed BL- α^+ borophene B_{22} ($Cmmm$) (3), and staggered BL- α^+ borophene B_{22} ($C2/m$) (4), graphene C_2 ($P6/mmm$) (5), and coronene D_{6h} $C_{24}H_{12}$ (6), with the lattice parameters and interlayer distances indicated. The inward-buckled boron atoms forming the interlayer B–B bonds are highlighted in blue.

3 Results and discussions

3.1 Structures and stability

B_{36} (1) is known to possess a perfect C_{6v} quasi-planar structure with a B_6 hexagon at the center surrounded by three concentric boron rings: the inner B_6 ring, middle B_{12} ring, and outer B_{18} ring (Fig. 1). Using B_{36} (1) as building blocks, the perfect planar ML- α^+ borophene B_{11} (2, $P6/mmm$) composed of edge-sharing B_{36} subunits in a honeycomb structure can be constructed. ML- α^+ borophene (2) consists of interwoven BTCs shared by neighboring B_{36} subunits, similar to the situation in ML graphene (5) which consists of CSCs shared by neighboring C_6 hexagons. Although ML- α^+ borophene (2) itself with dangling bonds in vertical direction is unstable both thermodynamically and kinetically, two such ML- α^+ borophenes can be assembled to form highly stable BL- α^+ borophenes: the eclipsed (A-A stacked) B_{22} (3, $Cmmm$) and staggered (A-B stacked) B_{22} (4, $C2/m$) with the interlayer B–B distance of 1.76 Å, which appear to be both thermodynamically and kinetically stable with the cohesive energies of $E_{coh} = -6.235$ and -6.238 eV/atom at GGA-PBE level, respectively ($E_{coh} = (E_{tot} - nE_B)/n$, where n is the number of boron atoms in the unit cell, E_{tot} the total energy of the unit cell, and E_B the energy of a free B atom in vacuum). The two close-lying BL- α^+ borophenes are practically iso-energetic in thermodynamics, with the slightly more stable A-B stacked B_{22} (4) constructed from BL B_{22} (3) via shifting the bottom layer by approximately one-third of the long diagonal of the unit cell ($\sqrt{3}/3a$, $\sqrt{3}/3b$), similar to the situation in the most stable A-B stacked BL graphene which features weak interlayer π – π stacking interactions. Both BL- α^+ borophenes B_{22} (3) and B_{22} (4) with the hole density of $\eta = 1/12$ and interlayer bonding density of $u = 1/4$ possess three interlayer B–B σ -bonds between six inward-buckled atoms in each unit cell which behave like three “pillars” nailing the top and bottom layers together. Interestingly, as indicated in Table 1, BL- α^+ borophenes B_{22} (3) and B_{22} (4) are more stable than all the BL borophenes reported to date in the literature. The previously reported close-packed BL borophenes B_{14} ($P6$) [55], B_{12} ($P6mmm$) [33], and B_8 ($Pmmm$) [32] appear to be 0.168, 0.129, and 0.050 eV/atom less stable in cohesive energies than BL B_{22} (3) and B_{22} (4) at PBE level, respectively. B_{22} (3) and B_{22} (4) also appear to be 0.031 and 0.034 eV/atom more favorable in cohesive energy than the previously reported BL borophene B_{30} ($Cmmm$) constructed from the experimentally observed B_{48}^{+0} [50, 51]. The BL- α borophene realized on Ag(111) substrate reported in Ref. [35] is found to be relaxed to the freestanding BL- α B_{16} ($P6/m2$) (Fig. S1(a) in the ESM) which has the low cohesive energy of $E_{coh} = -6.088$ eV/atom, a hole density of $\eta = 1/9$, and a halved interlayer bonding density of $u = 1/9$, while the supported BL borophene (P1) on Cu(111) observed in Ref. [36] has an even lower calculated cohesive energy of $E_{coh} = -6.057$ eV/atom when peeled off from the metal substrate (Fig. S1(b) in the ESM).

More encouragingly, extensive ATAT GM searches with the

Table 1 Space groups, lattice constants a and b , number of interlayer B–B bonds per unit cell ($N_{\text{B–B}}$), hole densities η , interlayer bonding density u , and cohesive energies per atom E_{coh} of bilayer borophenes reported in literature at GGB-PBE level. The most stable BL- α^+ B₂₂ (3) and BL B₂₂ (4) are tabulated in the last two rows for comparison

Phase	a (Å)	b (Å)	$N_{\text{B–B}}$	η	u	E_{coh} (eV/atom)
B ₁₄ (P6) [55]	4.36	4.36	3	—	3/7	-6.070
B ₁₆ BL a-sheet	5.00	5.00	1	1/9	1/9	-6.088
B ₆ (P6mmm) [33]	2.86	2.86	1	—	1/3	-6.109
B ₁₂ (C2/m) [33]	5.66	2.82	—	—	—	-6.176
B ₃₀ (P2/m) [56]	6.80	6.80	4	1/16	1/4	-6.178
B ₈ (Pmmm) [32]	2.86	3.24	2	—	1/4	-6.188
B ₃₀ (Cmmm) [56, 57]	6.60	6.60	4	1/16	1/4	-6.204
B ₂₂ (Cmmm)*	5.71	5.71	3	1/12	1/4	-6.235
B ₂₂ (C2/m)*	5.71	5.71	3	1/12	1/4	-6.238

Vac treated as dopants indicate that BL- α^+ B₂₂ (3) and BL B₂₂ (4) are the most stable BL borophenes obtained to date with the hole density ranging from $\eta = 0$ to $\eta = 0.25$, as clearly shown in Fig. 2. BL- α^+ B₂₂ (3) and BL- α^+ B₂₂ (4) have 2 vacancies in 24 lattice sites (B₂₂(Vac)₂) in each unit cell with the hole density of $\eta = 1/12$, while the third stable BL borophene B₃₀ (Cmmm) has 2 vacancies in 32 lattice sites (B₃₀(Vac)₂) with $\eta = 1/16$. The lowest-lying BL

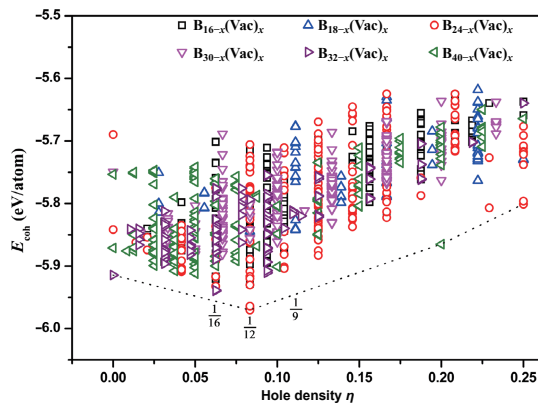


Figure 2 Average cohesive energies per atom E_{coh} of the bilayer borophenes obtained as a function of hole density η at PBE level.

configurations (Fig. S2 in the ESM) obtained via extensive structural searches based on the PSO approach implemented in CALYPSO appear to be in good agreement with the ATAT results discussed above, providing further evidence that BL- α^+ B₂₂ (3) and BL B₂₂ (4) are the most stable BL borophenes obtained to date.

As indicated in Fig. 3, both BL- α^+ B₂₂ (3) and BL- α^+ B₂₂ (4) exhibit no imaginary phonon modes on their phonon dispersion curves in the first Brillouin zones, indicating the high dynamic stability of these BL- α^+ borophenes. The calculated band structures in Fig. 3 show that they are semiconductors with the indirect band gaps of 0.952 and 1.144 eV at HSE06, respectively. For BL- α^+ B₂₂ (3), the conductance band minimum (CBM) is located at the C point while the valence band maximum (VBM) is slightly deviated from the Γ point; whereas for the BL- α^+ B₂₂ (4), the CBM is shifted to the Y point, while the location of VBM remains essentially unchanged. For both the bilayer borophenes, the CBM is primarily contributed by the B p_z orbitals, while the VBM is derived from a hybridized state of the B p_z and p_{x+y} orbitals (Fig. 3, right) as a result of the interlayer bonding formed in the two bilayers.

We also assess the dynamic stability of BL B₂₂ (3) by performing AIMD simulations at 1,000 K with a time step of 1 fs. The structural snapshot of a 2 × 2 supercell at 10 ps (Fig. S3 in the ESM) reveals that the semiconducting BL borophene is dynamically stable at high temperatures. In addition, we calculate the elastic constants, Young's modulus, and Poisson's ratios of the BL B₂₂ (3). The elastic constants of BL B₂₂ (3) c_{11} , c_{22} , and c_{12} are 407.80, 463.91 and 47.48 N/m, respectively. The Young's moduli along the a - and b -directions are 402.94 and 458.38 N/m, respectively. Compared with isotropic graphene (5) [58], the BL B₂₂ (3) is mechanically anisotropic with direction-dependent elastic properties. Its calculated Poisson ratios along the a - and b -directions are 0.10 and 0.12, respectively, slightly lower than the corresponding values of ML graphene (Table S1 in the ESM).

3.2 Bonding analyses

To better comprehend the high stabilities of these BL borophenes, we perform detailed bonding analyses using both the ELF and SSAdNDP approaches. ELF surfaces can be viewed as a contour picture in real space with ELF values ranging from 0 to 1. The top and side views of the ELF isosurfaces of BL B₂₂ (3) are displayed in Figs. S4(a) and S4(b) in the ESM with ELF = 0.8. There exist two

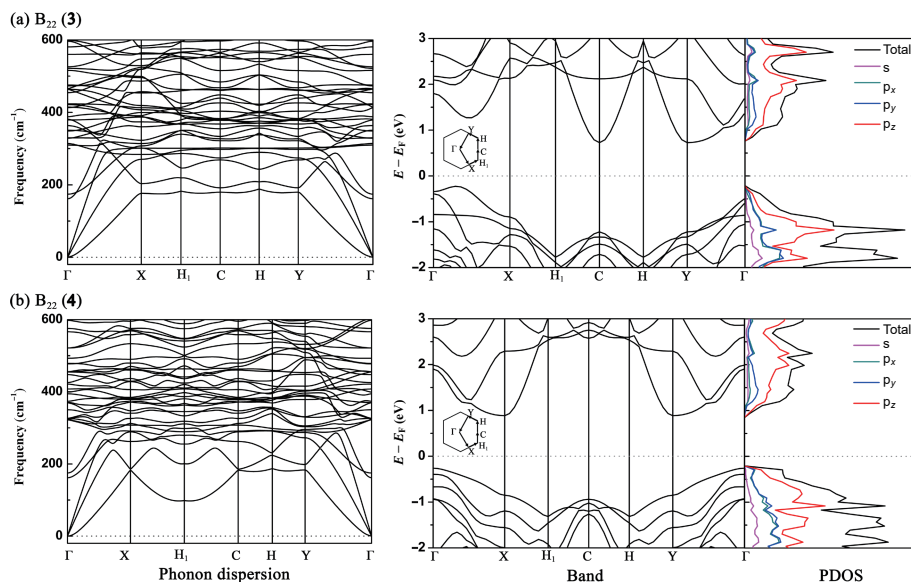


Figure 3 Calculated phonon dispersion spectra (at DFT-PBE) and band structures and projected densities of states (at HSE06) of the (a) eclipsed BL B₂₂ (3) and (b) staggered BL B₂₂ (4). The Fermi level is set to 0 eV.

electron localized areas in Figs. S4(a) and S4(b) in the ESM. One represents the delocalized in-plane σ -bonding interactions around the hexagonal holes on the top and bottom layers (Fig. S4(a) in the ESM), while the other shows the localized B–B σ -bonds on the B_2 pillars in between (Fig. S4(b) in the ESM). The sliced ELF distribution in Fig. S4(c) in the ESM again indicates that high ELF distributions exist at the middles of the pillars, corresponding to strong B–B σ -bonding interactions between the top and bottom layers. It is found from Fig. S4(d) in the ESM that ELF with 0.6 takes up most of the sliced plane at the bottom of the top layer. Figure S4(e) in the ESM again exhibits obvious electron delocalized areas around the hexagonal holes on both the top and bottom layers.

The SSAdNDP bonding patterns depicted in Figs. 4(a) and 4(b) provide a clearer and more specific description of the bonding interactions in BL B_{22} (3) and B_{22} (4). In each unit cell of BL- α^+ B_{22} (3) (Fig. 4(a)), there exist 3 localized B–B 2c-2e σ bonds with ON = 1.81–1.85 |e| on three B_2 pillars, 20 delocalized 3c-2e σ bonds with ON = 1.80–1.89 |e|, and 8 delocalized 4c-2e σ bonds with ON = 1.80–1.85 |e| evenly distributed on the top and bottom layers, forming a σ -framework with an overall point symmetry of D_{2h} in the unit cell. More interestingly, there have 2 delocalized 12c-2e π bonds with ON = 1.64 |e| symmetrically distributed around the two hexagonal holes on the top and bottom layers in each unit cell. BL- α^+ B_{22} (3) thus possesses one 12c-2e π bond over each hexagonal hole, similar to the situation in ML graphene (5) which contains one delocalized 6c-2e π bond over each C_6 hexagonal hole (Fig. 4(c)). The difference is that each 12c-2e π bond in semiconducting BL- α^+ B_{22} (3) shares one B atom with its neighbor, leaving two-thirds of the B-filled B_7 hexagons uncovered by delocalized π bonds, while each 6c-2e π bond in semimetallic ML graphene shares a C_2 edge with its neighbor, forming an even and continuous π -electron distribution over ML graphene (Fig. S5 in the ESM). Similar σ and π bonding patterns exist in BL- α^+ B_{22} (4) as shown in Fig. 4(b) where the delocalized 12c-2e π bond at the

bottom layer is shifted by one-third of the long diagonal of the unit cell, with the associated σ -framework shifted simultaneously in a concerted mechanism.

3.3 Supported BL- α^+ borophenes and three-dimensional borophites

Based on the most stable BL- α^+ B_{22} (3) and B_{22} (4) obtained, we explore the possibilities of forming supported BL- α^+ borophenes and three-dimensional (3D) α^+ -borophites (TD- α^+ borophites). As shown in Fig. 5, both BL- α^+ B_{22} (3) and B_{22} (4) exhibit marginal mismatch with the Ag(111) substrate in unit-cell geometries. The optimized lattice parameters of $a = b = 5.78 \text{ \AA}$ in the supported BL- α^+ borophenes match well with the experimentally measured $a = b = 5.7 \text{ \AA}$ for supported BL borophenes [35]. Such supported BL- α^+ borophenes possess the average cohesive energies per boron atom (defined as $E_{\text{coh}} = (E_{\text{tot}} - E_{\text{Ag}(111)} - nE_B)/n$, where $E_{\text{Ag}(111)}$ stands for the total energy of the Ag(111) substrate) of $E_{\text{coh}} = -6.340$ and -6.343 eV/atom , respectively. The average absorption energy per boron atom on the substrate is $E_{\text{abs}} = 0.105 \text{ eV/atom}$. With the calculated B–Ag distances of 2.2 \AA and slightly elongated interlayer B–B bond length of 1.8 \AA , the supported BL- α^+ borophenes are significantly more favorable in thermodynamics than the previously reported BL- α borophene [35] on Ag(111) which has $E_{\text{coh}} = -5.737 \text{ eV/atom}$ at the same theoretical level. These results present the possibility to form supported bilayer BL- α^+ borophenes on Ag(111) under suitable experimental conditions from which free-standing bilayer borophenes can be exfoliated from the substrate without obvious structural relaxations.

Extending BL- α^+ B_{22} (3) in vertical direction, the eclipsed TD- α^+ borophites B_{22} (*Cmmm*) (a) and staggered B_{44} (*C2/c*) (b) can be constructed which have the calculated cohesive energies of $E_{\text{coh}} = -6.254$ and -6.262 eV/atom respectively, suggesting that weak π – π stacking interactions (0.019 eV and 0.024 eV/atom, respectively) exist between neighboring BL- α^+ borophenes in these 3D structures (Fig. S6 in the ESM). The interlayer distance of 3.36 \AA in the slightly more stable staggered TD- α^+ B_{44} (b) is close to that

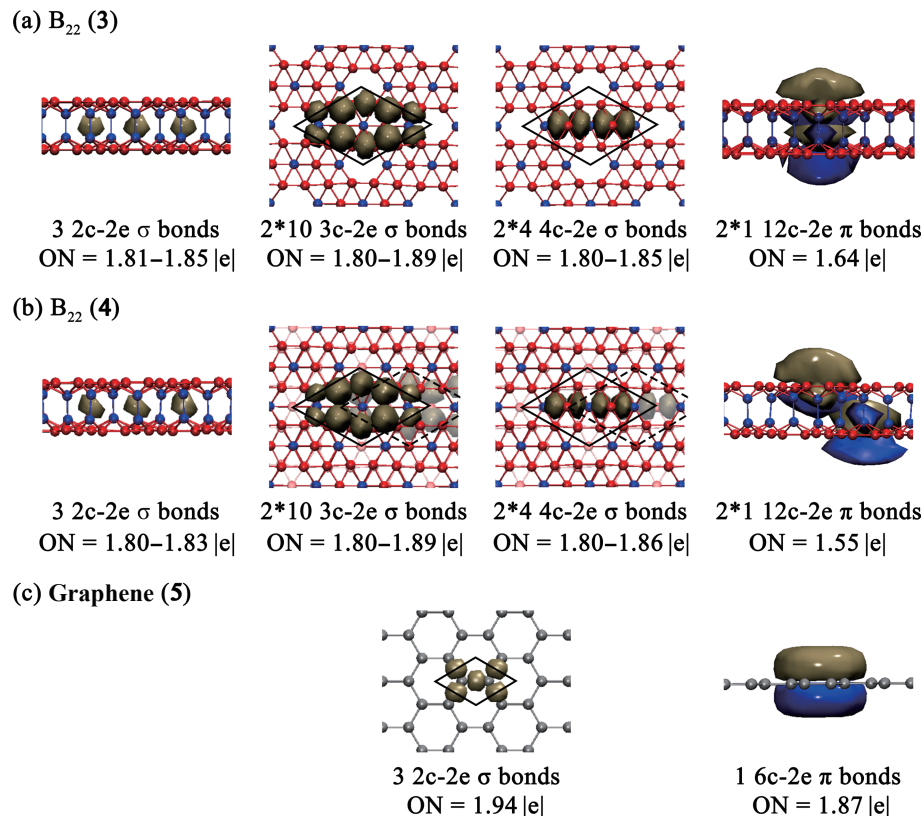


Figure 4 Comparison of the SSAdNDP bonding patterns of (a) BL- α^+ B_{22} (3), (b) B_{22} (4), and (c) ML graphene (5), with the occupations numbers (ONs) indicated.

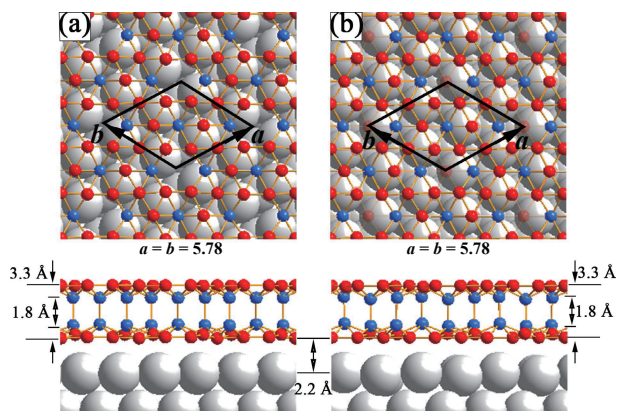


Figure 5 Top and side views of the supported (a) bilayer B_{22} (3) and (b) B_{22} (4) on Ag(111) substrate, with the inward-buckled boron atoms forming interlayer B–B σ bonds colored in blue and interlayer distances indicated in Å.

of 3.40 Å in graphite. However, AIMD simulations indicate that both these 3D TD- α^+ borophites are dynamically unstable at 300 K. They appear to be considerably less stable than the well-known α -rhombohedral boron which has the cohesive energy of $E_{coh} = -6.573$ eV/atom at PBE.

4 Conclusions

Based on extensive first-principles theory calculations in combination with extensive GM searches, we have presented in this work the two most stable BL- α^+ borophenes B_{22} (3) and B_{22} (4) reported to date which are indirect band gap semiconductors in nature. Chemical bonding analyses unveil the fact that strong interlayer B–B 2c-2e σ bonds help to stabilize these bilayer systems effectively and the delocalized 12c-2e π bonds over B_6 hexagonal holes in these semiconducting BL materials function similar to the delocalized 6c-2e π bonds over C_6 hexagons in semimetallic ML graphene. Such BL- α^+ borophenes match well with the Ag(111) substrate in lattice to form highly stable supported BL borophenes. These results offer new insights into structural chemistry of low-dimensional boron beyond the single-atomic-layer limit.

Acknowledgements

This work was supported by the National Natural Science Foundation of China (Nos. 21720102006, 21973057, 22073048, and 22003034). We sincerely thank Professor Boris Yakobson and Dr. Qiyuan Ruan at Rice University for inspiring discussions.

Electronic Supplementary Material: Supplementary material (optimized structures, molecular dynamical simulations, superatomic molecular orbitals, AdNDP bonding analyses, and optimized coordinates) is available in the online version of this article at <http://dx.doi.org/10.1007/s12274-022-4169-x>.

References

- [1] Novoselov, K. S.; Geim, A. K.; Morozov, S. V.; Jiang, D.; Zhang, Y.; Dubonos, S. V.; Grigorieva, I. V.; Firsov, A. A. Electric field effect in atomically thin carbon films. *Science* **2004**, *306*, 666–669.
- [2] Novoselov, K. S.; Geim, A. K.; Morozov, S. V.; Jiang, D.; Katsnelson, M. I.; Grigorieva, I. V.; Dubonos, S. V.; Firsov, A. A. Two-dimensional gas of massless dirac fermions in graphene. *Nature* **2005**, *438*, 197–200.
- [3] Cahangirov, S.; Topsakal, M.; Aktürk, E.; Şahin, H.; Ciraci, S. Two- and one-dimensional honeycomb structures of silicon and germanium. *Phys. Rev. Lett.* **2009**, *102*, 236804.
- [4] Feng, B. J.; Li, H.; Liu, C. C.; Shao, T. N.; Cheng, P.; Yao, Y. G.; Meng, S.; Chen, L.; Wu, K. H. Observation of dirac cone warping and chirality effects in silicene. *ACS Nano* **2013**, *7*, 9049–9054.
- [5] Vogt, P.; De Padova, P.; Quaresima, C.; Avila, J.; Frantzeskakis, E.; Asensio, M. C.; Resta, A.; Ealet, B.; Le Lay, G. Silicene: Compelling experimental evidence for graphenelike two-dimensional silicon. *Phys. Rev. Lett.* **2012**, *108*, 155501.
- [6] Kern, G.; Kresse, G.; Hafner, J. *Ab initio* calculation of the lattice dynamics and phase diagram of boron nitride. *Phys. Rev. B* **1999**, *59*, 8551–8559.
- [7] Song, L.; Ci, L.; Lu, H.; Sorokin, P. B.; Jin, C. H.; Ni, J.; Kvashnin, A. G.; Kvashnin, D. G.; Lou, J.; Yakobson, B. I. et al. Large scale growth and characterization of atomic hexagonal boron nitride layers. *Nano Lett.* **2010**, *10*, 3209–3215.
- [8] Wu, M. H.; Fu, H. H.; Zhou, L.; Yao, K. L.; Zeng, X. C. Nine new phosphorene polymorphs with non-honeycomb structures: A much extended family. *Nano Lett.* **2015**, *15*, 3557–3562.
- [9] Splendiani, A.; Sun, L.; Zhang, Y. B.; Li, T. S.; Kim, J.; Chim, C. Y.; Galli, G.; Wang, F. Emerging photoluminescence in monolayer MoS_2 . *Nano Lett.* **2010**, *10*, 1271–1275.
- [10] Radisavljevic, B.; Radenovic, A.; Brivio, J.; Giacometti, V.; Kis, A. Single-layer MoS_2 transistors. *Nat Nanotechnol* **2011**, *6*, 147–150.
- [11] Wang, L. S. Photoelectron spectroscopy of size-selected boron clusters: From planar structures to borophenes and borospherenes. *Int. Rev. Phys. Chem.* **2016**, *35*, 69–142.
- [12] Jian, T.; Chen, X. N.; Li, S. D.; Boldyrev, A. I.; Li, J.; Wang, L. S. Probing the structures and bonding of size-selected boron and doped-boron clusters. *Chem. Soc. Rev.* **2019**, *48*, 3550–3591.
- [13] Chen, Q.; Li, W. L.; Zhao, Y. F.; Zhang, S. Y.; Hu, H. S.; Bai, H.; Li, H. R.; Tian, W. J.; Lu, H. G.; Zhai, H. J. et al. Experimental and theoretical evidence of an axially chiral borospherene. *ACS Nano* **2015**, *9*, 754–760.
- [14] Zhai, H. J.; Zhao, Y. F.; Li, W. L.; Chen, Q.; Bai, H.; Hu, H. S.; Piazza, Z. A.; Tian, W. J.; Lu, H. G.; Wu, Y. B. et al. Observation of an all-boron fullerene. *Nat. Chem.* **2014**, *6*, 727–731.
- [15] Bezugly, V.; Kunstmänn, J.; Grundköetter-Stock, B.; Frauenheim, T.; Niehaus, T.; Cuniberti, G. Highly conductive boron nanotubes: Transport properties, work functions, and structural stabilities. *ACS Nano* **2011**, *5*, 4997–5005.
- [16] Mannix, A. J.; Zhou, X. F.; Kiraly, B.; Wood, J. D.; Alducin, D.; Myers, B. D.; Liu, X. L.; Fisher, B. L.; Santiago, U.; Guest, J. R. et al. Synthesis of borophenes: Anisotropic, two-dimensional boron polymorphs. *Science* **2015**, *350*, 1513–1516.
- [17] Decker, B. F.; Kasper, J. S. The crystal structure of a simple rhombohedral form of boron. *Acta Cryst.* **1959**, *12*, 503–506.
- [18] Li, W. L.; Chen, Q.; Tian, W. J.; Bai, H.; Zhao, Y. F.; Hu, H. S.; Li, J.; Zhai, H. J.; Li, S. D.; Wang, L. S. The B_{35} cluster with a double-hexagonal vacancy: A new and more flexible structural motif for borophene. *J. Am. Chem. Soc.* **2014**, *136*, 12257–12260.
- [19] Chen, Q.; Wei, G. F.; Tian, W. J.; Bai, H.; Liu, Z. P.; Zhai, H. J.; Li, S. D. Quasi-planar aromatic B_{36} and B_{36}^- clusters: All-boron analogues of coronene. *Phys. Chem. Chem. Phys.* **2014**, *16*, 18282–18287.
- [20] Piazza, Z. A.; Hu, H. S.; Li, W. L.; Zhao, Y. F.; Li, J.; Wang, L. S. Planar hexagonal B_{36} as a potential basis for extended single-atom layer boron sheets. *Nat. Commun.* **2014**, *5*, 3113.
- [21] Sergeeva, A. P.; Popov, I. A.; Piazza, Z. A.; Li, W. L.; Romanescu, C.; Wang, L. S.; Boldyrev, A. I. Understanding boron through size-selected clusters: Structure, chemical bonding, and fluxionality. *Acc. Chem. Res.* **2014**, *47*, 1349–1358.
- [22] Li, R.; You, X. R.; Wang, K.; Zhai, H. J. Nature of bonding in bowl-like B_{36} cluster revisited: Concentric $(6\pi + 18\pi)$ double aromaticity and reason for the preference of a hexagonal hole in a central location. *Chem. Asian J.* **2018**, *13*, 1148–1156.
- [23] Zhang, Z. H.; Penev, E. S.; Yakobson, B. I. Two-dimensional materials: Polyphony in B flat. *Nat. Chem.* **2016**, *8*, 525–527.
- [24] Tang, H.; Ismail-Beigi, S. Novel precursors for boron nanotubes: The competition of two-center and three-center bonding in boron sheets. *Phys. Rev. Lett.* **2007**, *99*, 115501.
- [25] Yang, X. B.; Ding, Y.; Ni, J. *Ab initio* prediction of stable boron sheets and boron nanotubes: Structure, stability, and electronic properties. *Phys. Rev. B* **2008**, *77*, 041402.
- [26] Penev, E. S.; Bhowmick, S.; Sadrzadeh, A.; Yakobson, B. I.

- Polymorphism of two-dimensional boron. *Nano Lett.* **2012**, *12*, 2441–2445.
- [27] Xu, S. G.; Li, X. T.; Zhao, Y. J.; Liao, J. H.; Xu, H.; Yang, X. B. An electron compensation mechanism for the polymorphism of boron monolayers. *Nanoscale* **2018**, *10*, 13410–13416.
- [28] Yu, X.; Li, L. L.; Xu, X. W.; Tang, C. C. Prediction of two-dimensional boron sheets by particle swarm optimization algorithm. *J. Phys. Chem. C* **2012**, *116*, 20075–20079.
- [29] Feng, B. J.; Zhang, J.; Zhong, Q.; Li, W. B.; Li, S.; Li, H.; Cheng, P.; Meng, S.; Chen, L.; Wu, K. H. Experimental realization of two-dimensional boron sheets. *Nat. Chem.* **2016**, *8*, 563–568.
- [30] Campbell, G. P.; Mannix, A. J.; Emery, J. D.; Lee, T. L.; Guisinger, N. P.; Hersam, M. C.; Bedzyk, M. J. Resolving the chemically discrete structure of synthetic borophene polymorphs. *Nano Lett.* **2018**, *18*, 2816–2821.
- [31] Zhang, Z. H.; Yang, Y.; Gao, G. Y.; Yakobson, B. I. Two-dimensional boron monolayers mediated by metal substrates. *Angew. Chem., Int. Ed.* **2015**, *54*, 13022–13026.
- [32] Zhou, X. F.; Dong, X.; Oganov, A. R.; Zhu, Q.; Tian, Y.; Wang, H. T. Semimetallic two-dimensional boron allotrope with massless dirac fermions. *Phys. Rev. Lett.* **2014**, *112*, 085502.
- [33] Ma, F. X.; Jiao, Y. L.; Gao, G. P.; Gu, Y. T.; Bilic, A.; Chen, Z. F.; Du, A. J. Graphene-like two-dimensional ionic boron with double dirac cones at ambient condition. *Nano Lett.* **2016**, *16*, 3022–3028.
- [34] Zhao, Y. C.; Zeng, S. M.; Ni, J. Superconductivity in two-dimensional boron allotropes. *Phys. Rev. B* **2016**, *93*, 014502.
- [35] Liu, X. L.; Li, Q. C.; Ruan, Q. Y.; Rahn, M. S.; Yakobson, B. I.; Hersam, M. C. Borophene synthesis beyond the single-atomic-layer limit. *Nat. Mater.* **2022**, *21*, 35–40.
- [36] Chen, C. Y.; Lv, H. F.; Zhang, P.; Zhuo, Z. W.; Wang, Y.; Ma, C.; Li, W. B.; Wang, X. G.; Feng, B. J.; Cheng, P. et al. Synthesis of bilayer borophene. *Nat. Chem.* **2022**, *14*, 25–31.
- [37] Van De Walle, A.; Asta, M.; Ceder, G. The alloy theoretic automated toolkit: A user guide. *Calphad* **2002**, *26*, 539–553.
- [38] Sanchez, J. M.; Ducastelle, F.; Gratias, D. Generalized cluster description of multicomponent systems. *Physica A: Stat Mech Appl* **1984**, *128*, 334–350.
- [39] Wang, Y. C.; Lv, J.; Zhu, L.; Ma, Y. M. Crystal structure prediction via particle-swarm optimization. *Phys. Rev. B* **2010**, *82*, 094116.
- [40] Perdew, J. P.; Burke, K.; Ernzerhof, M. Generalized gradient approximation made simple. *Phys. Rev. Lett.* **1996**, *77*, 3865–3868.
- [41] Kresse, G.; Furthmüller, J. Efficiency of *ab-initio* total energy calculations for metals and semiconductors using a plane-wave basis set. *Comput. Mater. Sci.* **1996**, *6*, 15–50.
- [42] Kresse, G.; Furthmüller, J. Efficient iterative schemes for *ab initio* total-energy calculations using a plane-wave basis set. *Phys. Rev. B* **1996**, *54*, 11169–11186.
- [43] Li, F. Y.; Jin, P.; Jiang, D. E.; Wang, L.; Zhang, S. B.; Zhao, J. J.; Chen, Z. F. B_{80} and $B_{101-103}$ clusters: Remarkable stability of the core–shell structures established by validated density functionals. *J. Chem. Phys.* **2012**, *136*, 074302.
- [44] Grimme, S. Semiempirical GGA-type density functional constructed with a long-range dispersion correction. *J. Comput. Chem.* **2006**, *27*, 1787–1799.
- [45] Savin, A.; Jepsen, O.; Flad, J.; Andersen, O. K.; Preuss, H.; Von Schnering, H. G. Electron localization in solid-state structures of the elements: The diamond structure. *Angew. Chem., Int. Ed.* **1992**, *31*, 187–188.
- [46] Silvi, B.; Savin, A. Classification of chemical bonds based on topological analysis of electron localization functions. *Nature* **1994**, *371*, 683–686.
- [47] Heyd, J.; Scuseria, G. E.; Ernzerhof, M. Hybrid functionals based on a screened Coulomb potential. *J. Chem. Phys.* **2003**, *118*, 8207–8215.
- [48] Parlinski, K.; Li, Z. Q.; Kawazoe, Y. First-principles determination of the soft mode in cubic ZrO_2 . *Phys. Rev. Lett.* **1997**, *78*, 4063–4066.
- [49] Togo, A.; Oba, F.; Tanaka, I. First-principles calculations of the ferroelastic transition between rutile-type and $CaCl_2$ -type SiO_2 at high pressures. *Phys. Rev. B* **2008**, *78*, 134106.
- [50] Gonze, X.; Lee, C. Dynamical matrices, born effective charges, dielectric permittivity tensors, and interatomic force constants from density-functional perturbation theory. *Phys. Rev. B* **1997**, *55*, 10355–10368.
- [51] Nosé, S. A unified formulation of the constant temperature molecular dynamics methods. *J. Chem. Phys.* **1984**, *81*, 511–519.
- [52] Nosé, S. A molecular dynamics method for simulations in the canonical ensemble. *Mol. Phys.* **1984**, *52*, 255–268.
- [53] Galeev, T. R.; Dunnington, B. D.; Schmidt, J. R.; Boldyrev, A. I. Solid state adaptive natural density partitioning: A tool for deciphering multi-center bonding in periodic systems. *Phys. Chem. Chem. Phys.* **2013**, *15*, 5022–5029.
- [54] Humphrey, W.; Dalke, A.; Schulten, K. VMD: Visual molecular dynamics. *J. Mol. Graph.* **1996**, *14*, 33–38.
- [55] Xu, S. G.; Zheng, B. B.; Xu, H.; Yang, X. B. Ideal nodal line semimetal in a two-dimensional boron bilayer. *J. Phys. Chem. C* **2019**, *123*, 4977–4983.
- [56] Chen, W. J.; Ma, Y. Y.; Chen, T. T.; Ao, M. Z.; Yuan, D. F.; Chen, Q.; Tian, X. X.; Mu, Y. W.; Li, S. D.; Wang, L. S. B_{48}^- : A bilayer boron cluster. *Nanoscale* **2021**, *13*, 3868–3876.
- [57] Gao, N.; Wu, X.; Jiang, X.; Bai, Y. Z.; Zhao, J. J. Structure and stability of bilayer borophene: The roles of hexagonal holes and interlayer bonding. *FlatChem* **2018**, *7*, 48–54.
- [58] Wei, X. D.; Fragneaud, B.; Marianetti, C. A.; Kysar, J. W. Nonlinear elastic behavior of graphene: *Ab initio* calculations to continuum description. *Phys. Rev. B* **2009**, *80*, 205407.